Pol. J. Environ. Stud. Vol. 31, No. 6 (2022), 5781-5792
DOI: *10.15244/pjoes/150386* ONLINE PUBLICATION DATE: 2022-10-03

Original Research

Removal Characteristics and Mechanism of Mn(II) from Acidic Wastewater Using Red Mud-Loess Mixture

Yisi Lu[1], Xiaofeng Liu[1], Liyuan Yu[1], Xidong Zhang[1], Wei Duan[1], Junboum Park[2], Xiaoqiang Dong[1]*

[1]College of Civil Engineering, Taiyuan University of Technology, No.79 West Yingze Street, Taiyuan, Shanxi, 030024, China
[2]Department of Civil and Environmental Engineering, Seoul National University, Gwanak-gu, Seoul, 08826, South Korea

Received: 9 March 2022
Accepted: 24 May 2022

Abstract

In this study, the feasibility of using red mud (RM)-loess (L) mixture (RM-L) to treat acidic wastewater (AW) containing Mn(II) was investigated through batch experiments. The optimum mass ratio of RM to L was obtained by exploring the treatment performance of varied mass ratios of RM to L on AW under different initial pH values. Furthermore, the effects of dosage, contact time, and initial concentration on the treatment of AW with RM-L under optimum mass ratio were explored. The removal mechanism of Mn(II) was clarified using adsorption mathematical models combined with characterization. The results indicate that the optimum mass ratio of RM to L was 7:3. The addition of L promotes the equilibrium adsorption for Mn(II) on RM-L under optimum mass ratio (RM-L (7:3)) and improves the dispersibility of RM-L (7:3). Moreover, hydroxyl, carbonate, and metal-oxygen groups in RM-L (7:3) play an important role in the removal of Mn(II) and the increase in pH value to 8.4 from 3. The adsorption type of Mn(II) is monolayer adsorption, and the adsorption process of Mn(II) is spontaneous and dominated by chemical adsorption.

Keywords: solid waste, synergistic purification, acid mine drainage, heavy mental ions, monolayer adsorption

Introduction

Safe and healthy water resources are the basis of human survival, but the actual water environment is experiencing severe challenges due to industrial production and human activities, which makes water resources have organic and inorganic pollution [1-5]. Acid mine drainage (AMD) is one of the three major ecological risks recognized by the United States Environmental Protection Agency [6]. AMD is formed by the oxidation of sulfide-containing minerals when they are exposed to oxygen and water

*e-mail: dongxiaoqiang@tyut.edu.cn

after mining [7, 8]. Whether mine wastewater is neutral or acidic depends on the pyrite content [9]. The AMD generated by mines in operation can be effectively controlled and treated at a low cost through human intervention. However, the problem of AMD generated by abandoned mines is challenging to the ecosystem [10, 11]. The AMD generated by abandoned coal mines cannot be effectively and properly treated and improved, so a large amount of Fe(II), Pb(II), Cu(II), Zn(II), Cd(II), Mn(II) and highly acidic wastewater directly enters groundwater and surface water, which produces extremely serious pollution in the ecological environment and triggers irreversible implications [12-14]. Therefore, the treatment of AMD has attracted worldwide attention.

At present, adding chemical neutralizers is the most widely accepted approach to treating AMD. Nevertheless, some disadvantages may exist in this method; for instance, the operating cost is high and a large amount of sludge may be generated and cause secondary pollution [15]. Thus, a material with good treatment efficiency and low cost should be urgently developed to treat AMD. Given its good adsorption capacity and environmentally friendly performance, solid waste has created a new chapter of resource utilization in the field of contaminated water and soil remediation [16-18].

Red mud (RM) is a type of general industrial solid waste generated from alumina production. In 2018, more than 105 million tons of RM were reserved in China [19]. An excess of RM may cause environmental pollution and safety hazards [20, 21]. Meanwhile, loess(L) is a type of aeolian sedimentary soil, especially the main distribution soil of Shanxi Province, which is a major coal-producing province in China [12, 22].

The use of RM to remove heavy metal ions in wastewater is one of the promising approaches for RM utilization, since RM has a good adsorption capacity for most heavy metal ions and a low cost [2, 16, 23-26]. RM should be dealkalized before it becomes an adsorbent because RM conventionally has alkalinity [27]. However, the direct use of RM to treat acidic wastewater containing heavy metal ions can reduce the treatment cost, considering that the alkalinity and adsorption capacity of RM will be effectively utilized [16]. There is a net positive synergism in mixing alkaline waste, i.e., RM, with AMD from an environmental perspective [28]. Nonetheless, in our preliminary experiment, a small amount of RM without dealkalization can easily make the pH value of the wastewater after treatment exceed the standard value when the removal sufficiency of heavy metal ions is not good, which is unfriendly to the environment. Therefore, we hope that other materials with good acidic buffering capacity and RM are used in combination to improve this situation. Chen et al. found that L had a certain buffering capacity for acidic solutions and rapid adsorption performance for heavy metals. And L possesses an excellent adsorption capacity for Pb(II), Cu(II), and Zn(II), but it has a poor adsorption capacity for Mn(II) [29-31]. As low-cost and abundant materials, RM and L also have complementary space in terms of performance in acidic wastewater treatment. In addition, studies on the adsorption characteristics and mechanism of mixed adsorbents have rarely been conducted.

Therefore, the purpose of this study is to obtain RM and L mixture (RM-L) as a novel adsorbent to treat acidic wastewater (AW) containing Mn(II). First, the optimum mass ratio of RM to L was determined by studying the treatment performance of varied mass ratios of RM-L on AW under different initial pH values. The evaluation indices included the pH value of AW after treatment and the removal efficiency of Mn(II). Second, the removal characteristic of RM-L under optimum mass ratio to Mn(II) from AW was explored by analyzing the effects of the dosage, contact time, and initial concentration. Third, the removal mechanism of RM-L under optimum mass ratio to Mn(II) from AW was investigated by studying the adsorption equilibrium isotherms, adsorption kinetics, and adsorption thermodynamics, in combination with the characterization of RM-L under optimum mass ratio tested by X-ray diffraction (XRD), Fourier transform infrared spectroscopy (FTIR) and scanning electron microscopy-energy dispersive spectroscopy (SEM-EDS).

Materials and Methods

Materials

RM belongs to Bayer RM with a red-brown color and was provided by Liulin Aluminum Factory (Shanxi, China). L belongs to the surface accumulation soil of the late Quaternary sediment (Q4), which was collected from approximately 4-5 m underground at a construction site in the Dongshan area of Taiyuan (Shanxi, China). The main chemical components of RM and L tested by S4 Pioneer X-ray fluorescence (Bruker, Massachusetts, USA) are provided in Table 1. RM

Table 1. Main chemical components of RM and L.

Component (%)	Al_2O_3	SiO_2	CaO	Na_2O	Fe_2O_3	TiO_2	MgO	K_2O	Others
RM	24.34	20.17	18.26	9.61	9.40	3.56	1.26	0.64	12.76
L	11.75	58.88	7.98	4.54	2.05	2.18	1.70	0.60	10.32

and L were oven-dried at 105ºC for 24 h and subsequently passed through a No. 200 sieve. The particle sizes of RM and L were tested by using a BT-9300HT laser particle size analyzer (BETTER, Dandong, China), and the cumulative sieve residue curve is shown in Fig. 1. The percentage of RM particles smaller than 5 μm was greater than 88.4%, while the percentage of L particles larger than 5 μm exceeded 84.5%.

AW containing Mn(II) was produced by dissolving the analytical reagent $MnSO_4 \cdot H_2O$ in distilled water in a laboratory. Dilute sulfuric acid was used to adjust the pH value of the AW to simulate the acidity of AMD. Manganese sulfate monohydrate ($MnSO_4 \cdot H_2O$) and sulfuric acid were purchased from Tianli Chemical Reagent Co., Ltd. (Tianjin, China).

Methods of Batch Experiment

Batch experiments were conducted by placing a series of 250 mL conical flasks (containing the simulated AW and a certain amount of RM-L) in an SHA-BA thermostatic water-bath shaker (Kewei, Beijing, China) with a shaking frequency of 150 rpm. The samples were filtered through a 0.45μm filter membrane-aquo system. Then, the concentrations of Mn(II) and the pH values of the samples were measured using Arcos ICP-OES (Spectro, Kleve, Germany) and FE-28 pH meter (Mettler Toledo, Zurich, Switzerland) respectively. To reduce the experimental errors and ensure the reliability of the results, all experiments were performed with two sets of parallel samples to obtain the average value. The removal efficiency, adsorption amount at equilibrium time, and adsorption amount at time t of RM-L were calculated using Eqs. (1), (2), and (3), respectively [32].

$$R=\frac{C_0\text{-}C_e}{C_0}\times 100\% \quad (1)$$

$$q_e=\frac{(C_0\text{-}C_e)V}{m} \quad (2)$$

$$q_t=\frac{(C_0\text{-}C_t)V}{m} \quad (3)$$

where R is the removal efficiency of Mn(II), %; C_0, C_e, and C_t are the initial concentrations, equilibrium concentrations, and concentrations at the t of Mn(II), respectively, mg/L; q_0 and q_1 are the adsorption amounts on RM-L of unit mass at the time of equilibrium and t, respectively, mg/g; m is the mass of RM-L, g; V is the volume of the simulated AW, L. (m/V is the dosage, g/L).

The optimum mass ratio of RM to L was determined by investigating the treatment performance of RM-L with different mass ratios (i.e., L [0:10], 3:7, 5:5, 7:3, and RM [10:0]) on AW under different initial pH values (i.e., 2, 3, 4, 5, and 6), 12 g/L dosages, 480 min contact time, 100 mg/L initial concentration, and 25ºC contact temperature.

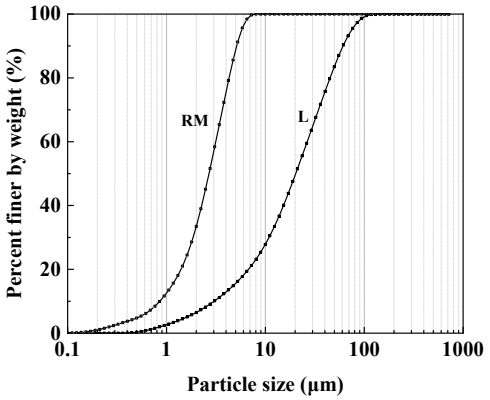

Fig. 1. Particle size distribution of RM and L.

The effects of dosage (i.e., 10, 12, 14, 16, and 18 g/L) on the treatment of AW with L, RM-L (7:3), RM were studied under the conditions of an initial pH value of 3, a contact time of 480 min, an initial concentration of 100 mg/L, and a contact temperature of 25ºC. The effects of contact time (i.e., 0, 20, 40, 60, 90, 120, 180, 240, 360, 480, and 600 min) on the treatment of AW with L, RM-L (7:3), RM were analyzed at an initial pH value of 3, a dosage of 12 g/L, an initial concentration of 100 mg/L, and a contact temperature of 25ºC. The effects of initial concentration (i.e., 25, 50, 100, 150, and 200 mg/L) on the treatment of AW at 25, 35 and 45ºC were explored using RM-L (7:3) at an initial pH value of 3, a dosage of 12 g/L, and a contact time of 480 min.

Moreover, the adsorption isotherms were obtained by analyzing the results of varying initial concentrations at 25ºC, the adsorption kinetics were obtained by studying the results of varying contact times at 25ºC, and the adsorption thermodynamics were obtained by investigating the results of varying initial concentrations at 25, 35, 45ºC.

Characterization of RM-L

The molecular structure of the samples was analyzed using a VERTEX70 Fourier transform infrared spectrometer (Bruker, Massachusetts, USA) with the KBr tablet method. The mineral phase of the samples was tested using a SmartLab X-ray diffractometer (Rigaku, Tokyo, Japan). The surface morphology and particle size of the samples were observed using a JSM-IT200 scanning electron microscope (JEOL, Tokyo, Japan).

Results and Discussion

Determination of the Optimum Mass Ratio of RM to L

Fig. 2 illustrates the effects of initial pH value (pH_0) and mass ratio of RM to L on the treatment

of AW. Fig. 2a) shows that the pH value of the AW after treatment was significantly increased by the presence of RM. In particular, the pH value of the AW after treatment with RM was significantly higher than those with other adsorbents. With the increase in initial pH value, the pH values of the AW after treatment with L stabilized at approximately 8.0, which indicates that L has a great buffering capacity for acidic solutions. This observation is consistent with other research [33], where alkaline substances such as calcite in L reacted with the acid in AW. The pH values of the AW after treatment with RM remained extremely high when the initial pH value exceeded 4; they could approach approximately 9.0, which is much higher than the standard limit value (GB/T 14848-2017, pH = 6.5-8.5) [34]. However, the pH values of AW after treatment by the other RM-L slightly changed under different initial pH values, which indicates that the buffering performance of RM-L to AW was improved once L was added.

Fig. 2b) illustrates the removal efficiency of Mn(II). The removal efficiency of Mn(II) was extremely low at a low initial pH value (pH_0 = 2), which was ascribed to the competing adsorption between hydrogen ions and heavy metals in the AW, which severely inhibited the adsorption of Mn(II) [35, 36]. The removal efficiency of Mn(II) was maintained in a stable range after the initial pH value exceeded 3, possibly due to the attenuation of competitive adsorption given the lower concentration of hydrogen ions in AW. RM greatly helped improve the removal capacity of RM-L for Mn(II). The presence of RM resulted in at least 11.1%-39.6% higher removal efficiencies for Mn(II) than that of L. The removal efficiency of Mn(II) first increased and gradually stabilized with the increase in the mass ratio of RM to L. The great adsorption response of RM improved the removal efficiency of RM-L for Mn(II). RM-L (7:3) and RM had an almost equal removal efficiency for Mn(II) when the initial pH value of AW was 2. This result demonstrates that the alkaline substances in L continued to react due to the presence of acidic substances in AW, which prevented hydrogen ions from occupying the adsorption sites. Consequently, the numerous adsorption sites and effective components of RM contributed to the removal of target ions and could make the pH value of AW after treatment close to neutral. At various initial pH values, with increasing mass ratio of RM to L, the pH values of AW continuously increased. Meanwhile, the removal efficiency of Mn(II) first increased and tended to stabilize when the mass ratio of RM to L exceeded 7:3. The pH value of the AW after treatment with RM was high, which might inhibit the wide utilization and development of RM-L. Accordingly, we conclude that the mass ratio of RM to L has an optimum solution in terms of pH value and removal efficiency in the treatment of AW containing Mn(II).

Therefore, the optimum mass ratio of RM to L was 7:3, and the RM-L under the optimum mass ratio (RM-L (7:3)) was selected to study the removal characteristics and mechanism of RM-L (7:3) in the following contents.

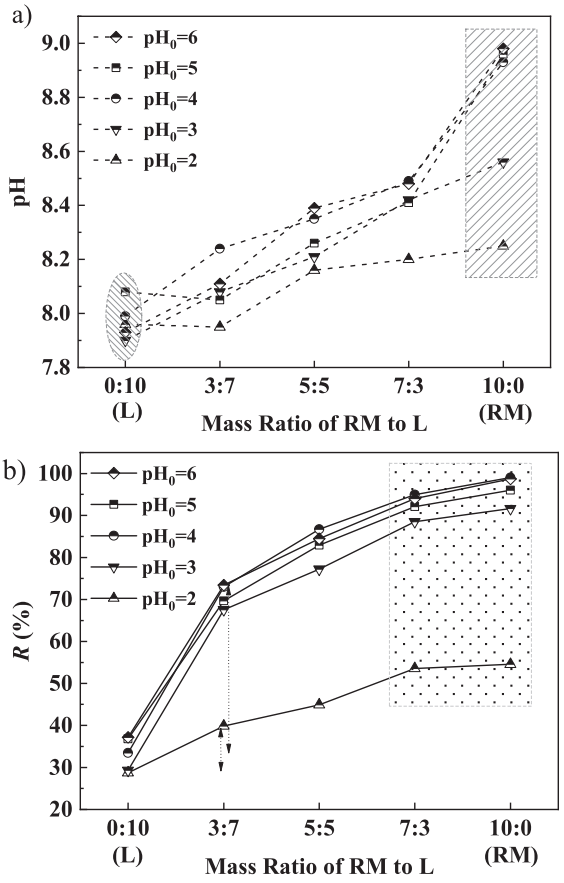

Fig. 2. Effect of mass ratio of RM to L on the treatment of AW under different initial pH values (pH_0) with RM-L: a) equilibrium pH value, b) removal efficiency (12 g/L, 480 min, 100 mg/L, 25ºC).

Removal Characteristics of RM-L (7:3)

Effect of Dosage

Fig. 3 shows the effect of dosage on the treatment of AW. The treatment effect of RM-L (7:3) was compared with those of RM and L.

Fig. 3a) presents that with the increase in dosage, the pH value of the AW after treatment with L was maintained at approximately 7.9. This result shows the great buffering capability of L to acidic solutions, and the alkaline substances released from L could be adjusted in accordance with the pH value of wastewater. For RM-L (7:3) and RM, the pH values of the AW after treatment increased with increasing dosage. This was due to the fact that RM does not have good adjustment and buffering capabilities for wastewater. Substantial alkaline substances were still released with the excessive dosage of the adsorbent under the condition that the concentration of Mn(II) was fixed, which caused the pH value of AW to be high. In particular, the pH value of

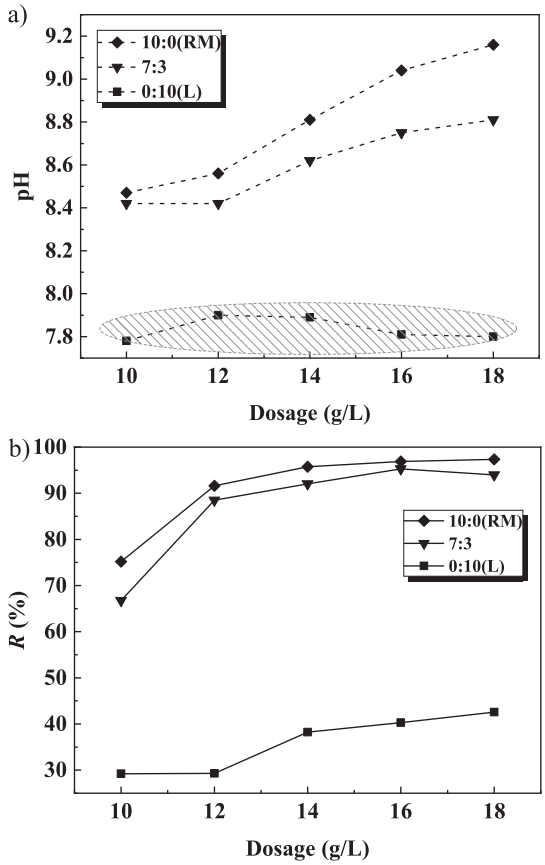

Fig. 3. Effect of dosage on the treatment of AW with RM-L: a) equilibrium pH value, b) removal efficiency (pH_0 = 3, 480 min, 100 mg/L, 25ºC).

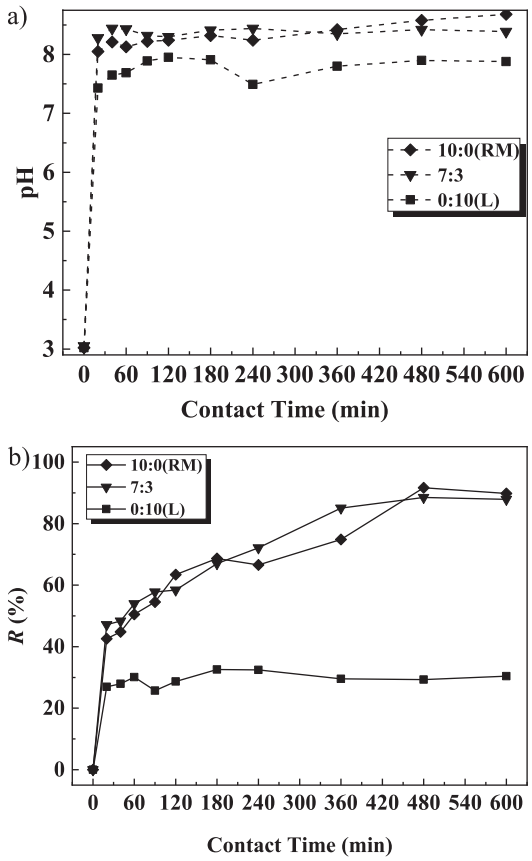

Fig. 4. Effect of contact time on the treatment of AW with RM-L: a) final pH value, b) removal efficiency (pH_0 = 3, 12 g/L, 100 mg/L, 25ºC).

the AW after treatment with RM significantly increased and exceeded 9.0.

Fig. 3b) shows the removal efficiencies of Mn(II) from AW using L, RM-L (7:3), and RM under different dosages. The addition of RM increased the removal efficiency of Mn(II) by at least 37.6%-59.2% compared with that of L. The removal efficiency of Mn(II) significantly increased and subsequently tended to stabilize with increasing dosage. The concentration of target ions that remained in AW was high when the dosage of RM-L was low, since the adsorption sites on RM-L were scarce relative to Mn(II) once the initial concentration was fixed and the driving force for the adsorption of target ions was low [37]. With the increase in dosage, the removal efficiency of Mn(II) was gradually enhanced owing to the increased adsorption sites of RM-L and increased alkalinity. The removal efficiency of Mn(II) eventually tended to stabilize because no more heavy metal ions were adsorbed on the excess adsorption sites when the initial concentration was fixed. Considering the pH value and removal efficiency, the optimum dosage of RM-L (7:3) for treating AW containing Mn(II) was 12 g/L. The pH value of AW after treatment was improved to 8.4 from 3, and the removal efficiency of Mn(II) was 88.5%.

Effect of Contact Time

Fig. 4 shows the effect of contact time on the AW treatment. The treatment effect of RM-L (7:3) was also compared with those of RM and L.

Fig. 4a) indicates that L, RM-L (7:3) and RM could be rapidly increased the pH value of AW to approximately 7.4, 8.3, and 8.1 from 3 at the initial stage (20 min), and finally reached 7.9, 8.4, 8.7. Fig. 4b) shows that the adsorption equilibriums of Mn(II) on RM-L (7:3) and RM both were reached at 480 min. Compared the fact that the equilibrium adsorption time for Mn(II) on L was 180 min, which indicates that L has the characteristic of rapid adsorption, as determined by Chen et al. [31]. The removal efficiency of Mn(II) by RM-L (7:3) reached 85.1% at 360 min, which was very close to the equilibrium removal efficiency of 88.5%.

The adsorption equilibrium trends of both RM-L (7:3) and RM for Mn(II) first increased and subsequently tended to be stable. The adsorption amount of Mn(II) sharply increased at the initial stage. Afterwards, an equilibrium was attained as time elapsed. The reason could be that the great concentration gradient of target ions between RM-L and AW made the mass transfer power large, and there were many unoccupied adsorption sites on RM-L in

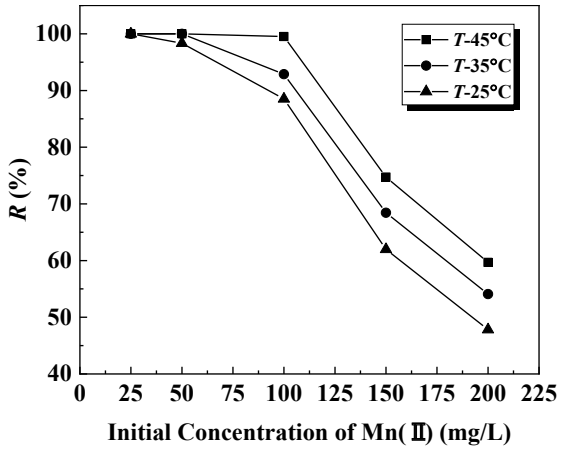

Fig. 5. Effect of initial concentration on the removal efficiency of Mn(II) from AW with RM-L (7:3) (pH_0 = 3, 12 g/L, 480 min, 25-45ºC).

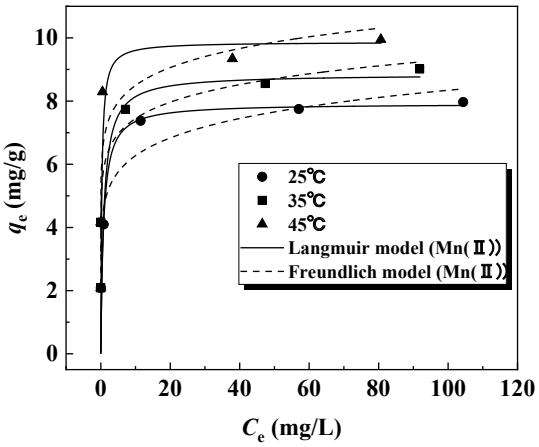

Fig. 6. Adsorption isotherm of Mn(II) adsorption on RM-L (7:3) (pH_0 = 3, 12 g/L, 480 min, 100 mg/L, 25-45ºC).

the initial stage [38, 39]. With the increase in contact time, the adsorption rates of Mn(II) decreased, and the removal efficiency eventually stabilized, possibly due to the decreased concentration difference between the solid-liquid interface and the saturated effective adsorption sites on RM-L. Therefore, the optimum contact time of RM-L (7:3) to treat AW containing Mn(II) was 480 min.

Effect of Initial Concentration

Fig. 5 shows the effect of initial concentration on the removal efficiency of Mn(II) from AW with RM-L (7:3) at 25, 35 and 45ºC. As shown in Fig. 5, when the initial concentration of Mn(II) was low, the removal efficiency of Mn(II) under the condition of a fixed dosage remained great, which resulted from the sufficient adsorption sites on RM-L (7:3) to accommodate the target ions; thus, Mn(II) was completely adsorbed. The removal efficiency of Mn(II) decreased from 100% to 47.8% when the initial concentration of Mn(II) increased from 25 to 200 mg/L. This result can be explained by the incomplete adsorption of Mn(II) in AW because the available adsorption sites on RM-L (7:3) were reduced [37], and the adsorption capacity gradually reached the limit. The removal efficiency of Mn(II) increased when the temperature increased, which proved that the high temperature benefited the adsorption of Mn(II) on RM-L (7:3).

Removal Mechanism of RM-L (7:3)

Adsorption Isotherms

The use of adsorption isotherms is one of the important approaches for studying the interaction between adsorbates and adsorbents.

Langmuir and Freundlich adsorption isotherms are shown in Eqs (4) and (5) [40].

$$q_e = \frac{q_m K_L C_e}{1 + K_L C_e} \quad (4)$$

$$q_e = K_F C_e^{\,n} \quad (5)$$

where q_m is the theoretical maximum adsorption capacity of the monolayer, mg/g; K_L is Langmuir constant, L/mg; n is the heterogeneity factor; and K_F is Freundlich constant, (mg/g)/(mg/L)^n.

We determined the adsorption process of Mn(II) on RM-L (7:3), specifically whether the adsorption type was favorable, by calculating the dimensionless equilibrium parameter from the Langmuir adsorption isotherm: $r = \frac{1}{1 + K_L C_0}$ [41].

Fig. 6 and Table 2 show the curve fitting results of the isotherm adsorption model of Mn(II) on RM-L (7:3) at 25, 35, and 45ºC. The results indicate that the adsorption isotherm models of RM-L (7:3) for Mn(II) fit well with the Langmuir adsorption isotherm model (R^2>0.9968). In the conditions of this study, r was 0.001-0.028, which suggests that RM-L (7:3) is beneficial to the adsorption of Mn(II), and has a high affinity and suitability for it. Moreover, n was 0.07-0.13, which was obtained by fitting the Freundlich adsorption isotherm with the experimental data. We can conclude that Mn(II) is beneficial to be adsorbed by RM-L (7:3) because the value of n is between 0 and 1 [42]. As a result, the adsorption of Mn(II) using RM-L (7:3) exhibited a better fit for the Langmuir adsorption isotherm than the Freundlich adsorption isotherms, indicating that the adsorption type of Mn(II) on RM-L (7:3) was monolayer adsorption.

Adsorption Kinetics

The rate-controlling steps of the adsorption process and adsorption mechanism were clarified by fitting the experimental data of Mn(II) on RM-L (7:3) to the pseudo-first-order kinetic model and

Table 2. Adsorption isotherm model fitting parameters for Mn(II) adsorption on RM-L (7:3).

T(ºC)	Langmuir model			Freundlich model		
	q_m (mg/g)	K_L (L/mg)	R^2	n	K_F (mg/g)/(mg/L)^n	R^2
25	7.98	1.39	0.9997	0.13	4.62	0.9650
35	8.97	2.03	0.9991	0.07	6.56	0.9968
45	9.87	3.61	0.9968	0.08	7.37	0.9707

pseudo-second-order kinetic model, as described in Eqs (6) and (7).

$$q_t=q_e(1-e^{-k_1 t}) \tag{6}$$

$$q_t=\frac{q_e^2 k_2 t}{1+q_e k_2 t} \tag{7}$$

where k_1 is the pseudo-first-order kinetic adsorption rate constant, min^{-1}; t is the adsorption time, min; and k_2 is the pseudo-second-order kinetic adsorption rate constant, g/mg/min.

The result of fitting the adsorption kinetic data of RM-L (7:3) to Mn(II) is shown in Fig. 7. The correlation coefficient of the pseudo-second-order kinetic of Mn(II) was 0.9183, indicating that the adsorption kinetics of Mn(II) by the RM-L (7:3) well fitted the pseudo-second-order kinetics. This result shows that chemical adsorption was the controlling step of the adsorption rate in the adsorption system [43-45]. The equilibrium adsorption capacity of Mn(II) estimated using the pseudo-second-order kinetic model was 7.27 mg/g, and the model-predicted value was in great agreement with the experimental data.

Adsorption Thermodynamics

The thermodynamic parameters were the Gibbs free energy change ΔG^θ, enthalpy change ΔH^θ and entropy change ΔS^θ. The standard Gibbs free energy change ΔG^θ is calculated using Eqs. (8), (9) and (10):

$$\Delta G^\theta=-RT\ln K_D \tag{8}$$

$$\Delta G^\theta=\Delta H^\theta-T\Delta S^\theta \tag{9}$$

$$\ln K_D=\frac{\Delta S^\theta}{R}-\frac{\Delta H^\theta}{RT} \tag{10}$$

where K_D is the thermodynamic equilibrium constant, dimensionless, and calculated by converting the units of K_L multiplied by the unitary standard concentration [46, 47]; ΔG^θ is the standard free energy change, kJ/mol; ΔH^θ is the enthalpy change, kJ/mol; and ΔS^θ is the entropy change, J/mol/K.

The adsorption thermodynamic parameters of Mn(II) were obtained through fitting the experimental data of RM-L (7:3) at 25, 35, and 45 °C. The results are shown in Fig. 8 and Table 3. From Table 3, ΔG^θ in the adsorption process of Mn(II) by RM-L (7:3) were negative at various contact temperatures. A higher temperature corresponds to a larger absolute value of ΔG^θ, indicating that the adsorption process of Mn(II) using RM-L (7:3) was spontaneous. The spontaneity was amplified with increasing temperature. ΔH^θ showed positive values during the adsorption process, illustrating that the adsorption process was endothermic. The adsorption performance of Mn(II) on RM-L (7:3)

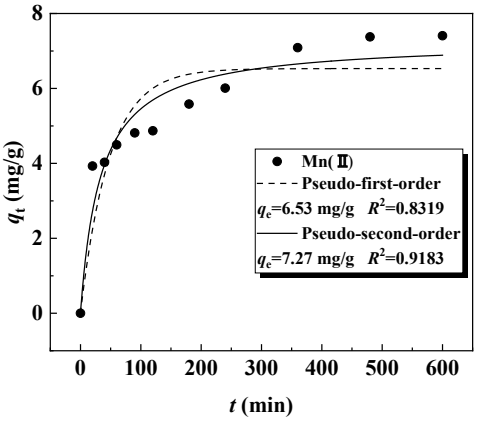

Fig. 7. Kinetic data and model for Mn(II) adsorption on RM-L (7:3) (pH_0 = 3, 12 g/L, 100 mg/L, 25ºC).

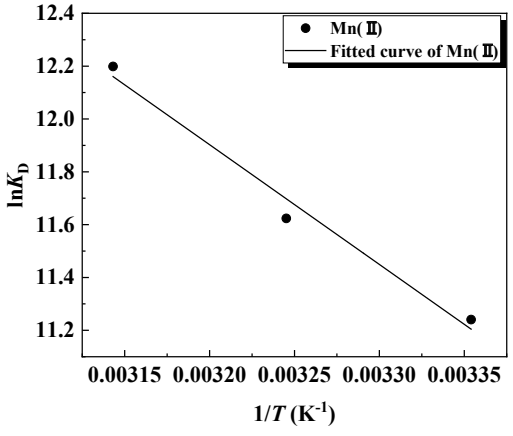

Fig. 8. Linear fit of thermodynamics for Mn(II) on RM-L (7:3) (pH_0 = 3, 12 g/L, 480 min, 25-200 mg/L, 25-45ºC).

Table 3. Adsorption thermodynamic parameters of Mn(II) adsorption on RM-L (7:3).

T (K)	K_D	ΔG^θ (kJ/mol)	ΔH^θ (kJ/mol)	ΔS^θ (J/mol/K)
298.15	76144.17	-27.86	37.69	219.58
308.15	111702.99	-29.78		
318.15	198532.74	-32.27		

was improved by the increase in temperature. ΔS^θ remained positive during the adsorption process. The entropy reduction caused by the adsorption of ions on RM-L (7:3) was less than the entropy addition caused by the desorption of other ions, so the total entropy in the entire adsorption process remained positive and the degrees of freedom of the solid–liquid interface increased [48].

XRD and FTIR

Fig. 9 depicts the XRD and FTIR spectra of RM, L, RM-L (7:3), and Mn(II)-loaded RM-L (7:3).

From Fig. 9a), the mineral phases of RM included katoite, silicatian ($Ca_3Al_2(SiO_4)(OH)_8$), hematite (Fe_2O_3), xonotlite ($Ca_6Si_6O_{17}(OH)_2$), and calcite ($CaCO_3$). The minerals of L included quartz (SiO_2), calcite ($CaCO_3$), gismondine ($CaAl_2Si_2O_8 4H_2O$), and a small amount of kaolinite ($Al(Si_4O_{10})(OH)_8$). No new minerals were generated after mixing RM and L. The peaks corresponding to calcite in RM-L (7:3) after the adsorption of Mn(II) weakened, and the peaks corresponding to katoite, silicatian and kaolinite weakened or changed, which indicates that calcite, katoite, silicatian and kaolinite contribute to the neutralization of acid and the removal of Mn(II) in AW.

From Fig. 9b), the stretching vibrations of hydroxyl group (-OH) were exhibited at wavenumbers of 3661, 3438 and 3429 cm^{-1}, whereas the bands at 1663, 1644 and 1618 cm^{-1} meant the bending of -OH from the water adsorbed onto the materials [17]. The peaks at 1437 cm^{-1}, 1444 cm^{-1}, and over 877 cm^{-1} correspond to carbonate group ($-CO_3$) stretching, which implies the presence of carbonate (i.e. calcite) in RM-L (7:3). The absorption peaks at 1000 cm^{-1} were assigned to the stretching vibration of Si-O-Si and Si-O-Al groups; the adsorption peaks at 696, 690, 612, 470, 457, and 451 cm^{-1} were caused by the vibration of Si-O and M-O groups (M stands for metal ion) [50].

The band of -OH was clearly stronger than that of L and the $-CO_3$ band was stronger than that of RM after mixing RM and L. The peaks of $-CO_3$ weakened as the adsorption was completed, which was probably because calcite in RM-L (7:3) greatly contributed to neutralizing the acid in AW. The peak of -OH moved from 3438 cm^{-1} to 3429 cm^{-1}, which was related to the stretching vibration of -OH, which indicates that Mn(II) successfully combined with -OH. And the M-O group

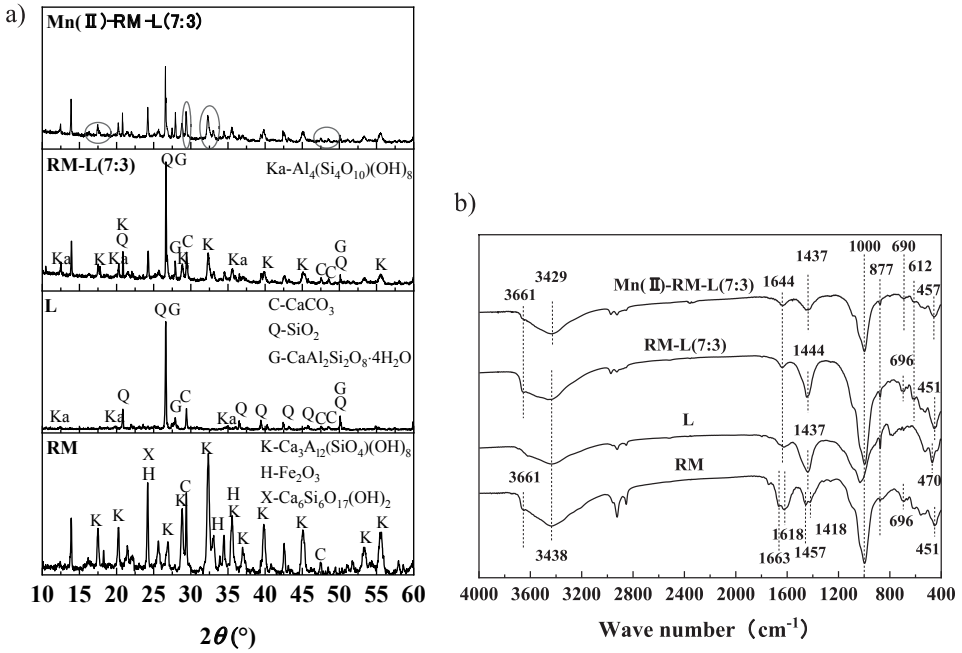

Fig. 9. XRD and FTIR spectra of RM, L, RM-L (7:3) and Mn(II)-loaded RM-L (7:3): a) XRD, b) FTIR (pH_0 = 3, 12 g/L, 600 min, 100 mg/L, 25ºC).

as potential binding sites made the main contribution to the removal of Mn(II) [51, 52]. Some complexes related to Mn(II) could be formed through reaction with aluminosilicate minerals and complexation reaction of kaolinite minerals in RM-L (7:3). The interaction between RM-L (7:3) and Mn(II) could be shown in Eqs (11) and (12).

$$CaCO_3 + 2H^+ \rightarrow CO_2 + H_2O + Ca^{2+} \quad (11)$$

$$\equiv XOH + Mn^{2+} \rightarrow \equiv XOMn^+ + H^+ \quad (12)$$

where X represents the clay mineral constituents in RM-L (7:3).

SEM-EDS

The surface morphology of RM, L, RM-L (7:3) before and after adsorption was observed and characterized using an electron microscope at a magnification of 5000 times. Fig. 10 shows the SEM images of RM, L, RM-L (7:3) and Mn(II)-loaded RM-L (7:3).

From Fig. 10a) and Fig. 10b), RM particles easily agglomerate, since most of the RM particles are less than 5 μm, but L has a relatively large particle size because the main minerals of L are calcite and quartz. The RM particles were homogeneously distributed in a finer state, as shown in Fig. 10c). The dispersibility

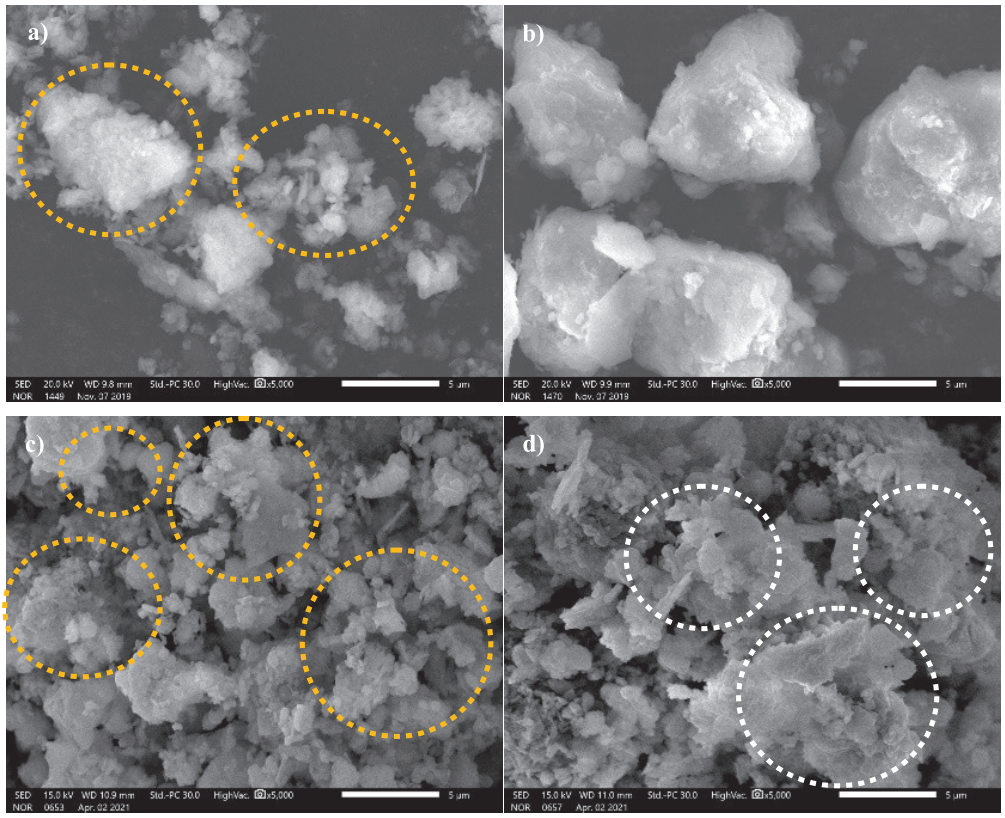

Fig. 10. SEM images of: a) RM, b) L, c) RM-L (7:3), d) Mn(II)-loaded RM-L (7:3) (pH_0 = 3, 12 g/L, 600 min,100 mg/L, 25ºC).

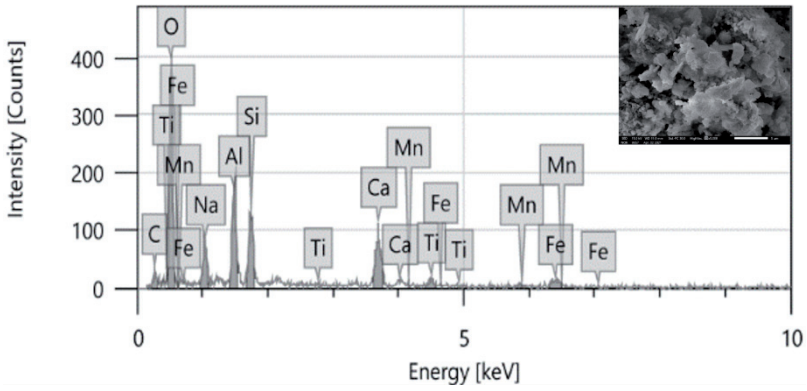

Fig. 11. EDS spectrum of Mn(II)-loaded RM-L (7:3) (pH_0 = 3, 12 g/L, 600 min, 100 mg/L, 25ºC).

of RM considerably improved after the RM and L were mixed, which was undoubtedly beneficial to the treatment capacity of RM-L (7:3) for AW in terms of pH value and removal efficiency. This result ensures that RM-L (7:3) and the heavy metal ions in the AW were fully contacted.

Fig. 10d) depicts that the protrusions on the surface of RM-L (7:3) were dissolved, the surface tended to be smooth, the pores tended to be filled, and the structure became dense due to the dissolution by acid and the adsorption of heavy metals. Fig. 11 shows the EDS spectrum of Mn(II)-loaded RM-L (7:3). The mass ratio of Mn(II) detectedby the corresponding EDS spectrum was 1.9%, which demonstrates the effectiveness and success of the adsorption.

Conclusions

The feasibility of treating AW with a mixture of solid waste RM and L was systematically investigated by evaluating the pH value and removal efficiency. The optimum mass ratio of RM to L was determined to be 7:3. Compared with the removal efficiency and buffering capacity of RM and L, those of RM-L (7:3) for the Mn(II) could be enhanced by combining RM and L. L provided a certain promoting ability to reduce the equilibrium time for Mn(II) adsorption on RM-L (7:3). Furthermore, the particles of RM-L (7:3) presented good dispersibility. The AW with an initial pH value of 3 and an initial concentration of 100 mg/L was treated with RM-L (7:3) at a dosage of 12 g/L, a contact time of 480 min, and a contact temperature of 25ºC, the pH value of the AW containing Mn(II) after treatment increased to 8.4 from 3, and the removal efficiency of Mn(II) was 88.5%. The adsorption of Mn(II) on RM-L (7:3) conformed to the Langmuir adsorption isotherm and pseudo-second-order kinetics. Therefore, the adsorption type of Mn(II) was monolayer adsorption, and the adsorption process was mainly chemical adsorption and a spontaneous endothermic process. The calcite, aluminosilicate minerals, and kaolinite minerals in RM-L (7:3) played an important role in the removal of Mn(II).

Therefore, the combination of RM and L provides a cost-effective and promising AMD treatment approach, and it is a far-reaching move for utilizing large amounts of RM. In the future, we should consider the competitive adsorption of other interfering ions in competitive systems and the stability of Mn(II) on Mn(II)-loaded RM-L (7:3) under complex conditions.

Acknowledgments

This study was financially supported by the National Natural Science Foundation of China (grant number: 51978438), the Natural Science Foundation of Shanxi (grant number: 202103021223122), and the National Research Foundation of Korea (grant number: 2021R1A2C201118012). The first author is also grateful to the China Scholarship Council for providing the joint Ph.D. studentship.

Conflict of Interest

The authors declare no conflict of interest.

References

1. NAUSHAD M., SHARMA G., ALOTHMAN Z.A. Photodegradation of toxic dye using Gum Arabic-crosslinked-poly(acrylamide)/$Ni(OH)_2$/FeOOH nanocomposites hydrogel. Journal of Cleaner Production, **241**, 118263, **2019**.
2. ALI I., ALHARBI O.M.L., ZA A.L., AL-MOHAIMEED A.M., ALWARTHAN A. Modeling of fenuron pesticide adsorption on CNTs for mechanistic insight and removal in water. Environmental Research, **170**, 389, **2019**.
3. WABAIDUR S.M., KHAN M.A., SIDDIQUI M.R., OTERO M., JEON B.-H., ALOTHMAN Z.A., HAKAMI A.A.H. Oxygenated functionalities enriched MWCNTs decorated with silica coated spinel ferrite – A nanocomposite for potentially rapid and efficient de-colorization of aquatic environment. Journal of Molecular Liquids, **317**, 113916, **2020**.
4. ALOTHMAN Z.A., BAHKALI A.H., KHIYAMI M.A., ALFADUL S.M., WABAIDUR S.M., ALAM M., ALFARHAN B.Z. Low cost biosorbents from fungi for heavy metals removal from wastewater. Separation Science and Technology, **55** (10), 1766, **2020**.
5. ALOTHMAN Z. A review: Fundamental aspects of silicate mesoporous materials. Materials, **5** (12), 2874, **2012**.
6. MOODLEY I., SHERIDAN C.M., KAPPELMEYER U., AKCIL A. Environmentally sustainable acid mine drainage remediation: Research developments with a focus on waste/by-products. Minerals Engineering, **126**, 207, **2018**.
7. MAKHATHINI T.P., MULOPO J., BAKARE B.F. Possibilities for acid mine drainage co-treatment with other waste streams: A review. Mine Water and the Environment, **39** (1), 13, **2020**.
8. NúñEZ-GóMEZ D., RODRIGUES C., LAPOLLI F.R., LOBO-RECIO M.Á. Adsorption of heavy metals from coal acid mine drainage by shrimp shell waste: Isotherm and continuous-flow studies. Journal of Environmental Chemical Engineering, **7** (1), 102787, **2019**.
9. TIWARY R.K. Environmental impact of coal mining on water regime and its management. Water, Air, and Soil Pollution, **132**, 185, **2001**.
10. NAIDU G., RYU S.C., THIRUVENKATACHARI R., CHOI Y.K., JEONG S.H., VIGNESWARAN S. A critical review on remediation, reuse, and resource recovery from acid mine drainage. Environmental Pollution, **247**, 1110, **2019**.
11. KHOEURN K., SAKAGUCHI A., TOMIYAMA S., IGARASHI T. Long-term acid generation and heavy metal leaching from the tailings of Shimokawa mine, Hokkaido, Japan: Column study under natural condition. Journal of Geochemical Exploration, **201**, 1, **2019**.

12. WANG Z.L., XU Y.X., ZHANG Z.X., ZHANG Y.B. Review: Acid mine drainage (AMD) in abandoned coal mines of Shanxi, China. Water, **13** (8), 1-21, **2020**.
13. JOHNSON D.B., HALLBERG K.B. Acid mine drainage remediation options: a review. Science of the Total Environment, **338** (1-2), 3, **2005**.
14. RODRíGUEZ-GALÁN M., BAENA-MORENO F.M., VáZQUEZ S., ARROYO-TORRALVO F., VILCHES L.F., ZHANG Z.E. Remediation of acid mine drainage. Environmental Chemistry Letters, **17** (4), 1529, **2019**.
15. IGARASHI T., HERRERA P.S., UCHIYAMA H., MIYAMAE H., IYATOMI N., HASHIMOTO K., TABELIN C.B. The two-step neutralization ferrite-formation process for sustainable acid mine drainage treatment: Removal of copper, zinc and arsenic, and the influence of coexisting ions on ferritization. Science of the Total Environment, **715**, 136877, **2020**.
16. KOMNITSAS K., BARTZAS G., PASPALIARIS I. Efficiency of limestone and red mud barriers: Laboratory column studies. Minerals Engineering, **17** (2), 183, **2004**.
17. KHAN T.A., CHAUDHRY S.A., ALI I. Equilibrium uptake, isotherm and kinetic studies of Cd(II) adsorption onto iron oxide activated red mud from aqueous solution. Journal of Molecular Liquids, **202**, 165, **2015**.
18. LI Y.C., HUANG H., XU Z., MA H.Q., GUO Y.F. Mechanism study on manganese(II) removal from acid mine wastewater using red mud and its application to a lab-scale column. Journal of Cleaner Production, **253**, 119955, **2020**.
19. WANG M.F., LIU X.M. Applications of red mud as an environmental remediation material: A review. Journal of Hazardous Materials, **408**, 124420, **2021**.
20. DANIEL W., ANDRAS B., BERNADETT B.-V., ÁDÁM E., ADRIENN H. Long-term ecological effects of the red mud disaster in Hungary: Regeneration of red mud flooded areas in a contaminated industrial region. Science of the Total Environment, **644**, 1292, **2018**.
21. LIU J., XIE Y., LI C., FANG G.T., CHEN Q.L., AO X.Q. Novel red mud/polyacrylic composites synthesized from red mud and its performance on cadmium removal from aqueous solution. Journal of Chemical Technology & Biotechnology, **95** (1), 213, **2019**.
22. LI Y.R., HE S.D., DENG X.H., XU Y.X. Characterization of macropore structure of Malan loess in NW China based on 3D pipe models constructed by using computed tomography technology. Journal of Asian Earth Sciences, **154**, 271, **2018**.
23. ZIJLSTRA J.J., DESSI R., PERETTI R., ZUCCA A. Treatment of percolate from metal sulfide mine tailings with a permeable reactive barrier of transformed red mud. Water Environment Research, **82** (4), 319, **2010**.
24. AZHAR A., YAMAUCHI Y., ALLAH A.E., ALOTHMAN Z.A., BADJAH A.Y., NAUSHAD M., HABILA M., WABAIDUR S., WANG J., ZAKARIA M. B. Nanoporous iron oxide/carbon composites through in-situ deposition of prussian blue nanoparticles on graphene oxide nanosheets and subsequent thermal treatment for supercapacitor applications. Nanomaterials, **9** (5), 776, **2019**.
25. ALQADAMI A.A., KHAN M.A., SIDDIQUI M.R., ALOTHMAN Z.A. Development of citric anhydride anchored mesoporous MOF through post synthesis modification to sequester potentially toxic lead (II) from water. Microporous and Mesoporous Materials, **261**, 198, **2018**.
26. MITTAL A., NAUSHAD M., MITTAL A., ALOTHMAN Z.A., WABAIDUR S.M., ALAM M. Fabrication of MWCNTs/ThO_2 nanocomposite and its adsorption behavior for the removal of Pb(II) metal from aqueous medium. Desalination and Water Treatment **57** (46), 21863, **2016**.
27. PIETRELLI L., IPPOLITO N.M., FERRO S., DOVI V.G., VOCCIANTE M. Removal of Mn and As from drinking water by red mud and pyrolusite. Journal of Environmental Management, **237**, 526, **2019**.
28. LUCAS H., STOPIC S., XAKALASHE B., NDLOVU S., FRIEDRICH B. Synergism red mud-acid mine drainage as a sustainable solution for neutralizing and immobilizing hazardous elements. Metals, **11** (620), 1, **2021**.
29. WANG Y., TANG X.W., LIU J.J., WANG H.Y., SUN Z.F. Adsorption behavior and mechanism of loess soil towards manganese ions. Chinese Journal of Geotechnical Engineering, **34** (12), 2292, **2012**.
30. Li Z.Z. Mechanism of sorption, desorption, diffusion and remediation of heavy metals in soils. Zhejiang University, China, **2009**.
31. CHEN Y.M., WANG Y.Z., XIE H.J., JIANG Y.S. Adsorption characteristics of loess-modified natural silt towards Pb(II): equilibrium and kinetic tests. Chinese Journal of Geotechnical Engineering, **36** (7), 1185, **2014**.
32. KENAWY E.R., GHFAR A.A., WABAIDUR S. M., KHAN M.A., SIDDIQUI M.R., ALOTHMAN Z.A., ALQADAMI A.A., HAMID M. Cetyltrimethylammonium bromide intercalated and branched polyhydroxystyrene functionalized montmorillonite clay to sequester cationic dyes. Journal of Environmental Management, **219**, 285, **2018**.
33. TANG X.W., LI Z.Z., CHEN Y.M. Behaviour and mechanism of Zn(II) adsorption on Chinese loess at dilute slurry concentrations. Journal of Chemical Technology & Biotechnology, **83** (5), 673, **2008**.
34. Standard for groundwater quality, Standardization Administration in China, China, **2017**.
35. TANG X.W., LI Z.Z., CHEN Y.M., WANG Z.Q. Removal of Zn(II) from aqueous solution with natural Chinese loess: Behaviors and affecting factors. Desalination, **249** (1), 49, **2009**.
36. ZHANG X.Y., LIU Y. Concurrent removal of Cu(II), Co(II) and Ni(II) from wastewater by nanostructured layered sodium vanadosilicate: Competitive adsorption kinetics and mechanisms. Journal of Environmental Chemical Engineering, **9** (5), 105945, **2021**.
37. AYALA J., FERNáNDEZ B. Treatment from abandoned mine landfill leachates. Adsorption technology. Journal of Materials Research and Technology, **8** (3), 2732, **2019**.
38. LIU G., XU L.S., LI Z.K., HUANG Q.Q., XIE Z.W., XU X.F. Adsorption of cadmium on hydroxyapatite/bentonite composites in aqueous solution. Journal of the Chinese Ceramic Society, **46** (10), 1414, **2018**.
39. NARAYANAN S.L., VENKATESAN G., POTHEHER I.V. Equilibrium studies on removal of lead (II) ions from aqueous solution by adsorption using modified red mud. International Journal of Environmental Science and Technology, **15** (8), 1687, **2018**.
40. KHAN M.A., ALQADAMI A.A., WABAIDUR S.M., SIDDIQUI M.R., JEON B.H., ALSHAREEF S.A., ALOTHMAN Z.A., HAMEDELNIEL A.E. Oil industry waste based non-magnetic and magnetic hydrochar to sequester potentially toxic post-transition metal ions from water. Journal of Hazardous Materials, **400**, 123247, **2020**.
41. MOHAN S., KUMAR V., SINGH D.K., HASAN S.H. Effective removal of lead ions using graphene

oxide-MgO nanohybrid from aqueous solution: Isotherm, kinetic and thermodynamic modeling of adsorption. Journal of Environmental Chemical Engineering, **5** (3), 2259, **2017**.
42. SADEGHALVAD B., AZADMEHR A.R., MOTEVALIAN H. Statistical design and kinetic and thermodynamic studies of Ni(II) adsorption on bentonite. Journal of Central South University, **24** (7), 1529, **2017**.
43. SHEN Z.T., JIN F., WANG F., MCMILLAN O., AL-TABBAA A. Sorption of lead by Salisbury biochar produced from British broadleaf hardwood. Bioresource Technology, **193**, 553, **2015**.
44. ZHANG Y.H., JIN F., SHEN Z.T., LYNCH R., AL-TABBAA A. Kinetic and equilibrium modelling of MTBE (methyl tert-butyl ether) adsorption on ZSM-5 zeolite: Batch and column studies. Journal of Hazardous Materials, **347**, 461, **2018**.
45. FAN S.S., WANG Y., WANG Z., TANG J., TANG J., LI X.D. Removal of methylene blue from aqueous solution by sewage sludge-derived biochar: Adsorption kinetics, equilibrium, thermodynamics and mechanism. Journal of Environmental Chemical Engineering, **5** (1), 601, **2017**.
46. LIMA E.C., HOSSEINI-BANDEGHARAEI A., MORENO-PIRAJáN J.C., ANASTOPOULOS I. A critical review of the estimation of the thermodynamic parameters on adsorption equilibria. Wrong use of equilibrium constant in the Van't Hoof equation for calculation of thermodynamic parameters of adsorption. Journal of Molecular Liquids, **273**, 425, **2019**.
47. GHOSAL P.S., GUPTA A.K. Determination of thermodynamic parameters from Langmuir isotherm constant-revisited. Journal of Molecular Liquids, **225**, 137, **2017**.
48. KUL A.R., KOYUNCU H. Adsorption of Pb(II) ions from aqueous solution by native and activated bentonite: kinetic, equilibrium and thermodynamic study. Journal of Hazardous Materials, **179** (1-3), 332, **2010**.
49. DEIHIMI, N., IRANNAJAD, M., REZAI, B. Equilibrium and kinetic studies of ferricyanide adsorption from aqueous solution by activated red mud. Journal of Environmental Management, **227**, 277, **2018**.
50. TSAMO C., DJOMOU DJONGA P.N., DANGWANG DIKDIM J.M., KAMGA R. Kinetic and equilibrium studies of Cr(VI), Cu(II) and Pb(II) removal from aqueous solution using red mud, a low-cost adsorbent. Arabian Journal for Science and Engineering, **43**, 2353, **2018**.
51. WU C., HUANG L., XUE S.G., HUANG Y.Y., HARTLEY W., CUI M.Q., WONG M.H. Arsenic sorption by red mud-modified biochar produced from rice straw. Environmental Science and Pollution Research **24** (22), 18168, **2017**.